

Article

Cyclic Behavior of High-Strength Lightweight Concrete Exterior Beam-Column Connections Reinforced with GFRP

Mahmoud A. El-Mandouh ^{1,*}, Mostafa. S. Omar ², Mohamed A. Elnaggar ³ and Ahmed S. Abd El-Maula ^{4,5}¹ Civil Construction Department, Beni-Suef University, Beni-Suef 62511, Egypt² Higher Institute for Engineering and Technology, Department of Structural Engineering, Behira 22511, Egypt; eng_mostfa_omar@hotmail.com³ Structural Engineering Department, Faculty of Engineering, Alexandria University, Alexandria 21519, Egypt; elnaggar_1974@yahoo.com⁴ Faculty of Engineering, Delta University for Science and Technology, Gamasa 35712, Egypt; ahmed.alsayed@feng.bu.edu.eg⁵ Shoubra Faculty of Engineering, Benha University, Benha 13511, Egypt

* Correspondence: mahmoudaziz_2008@yahoo.com

Abstract: Using lightweight reinforced concrete beams with glass fiber bars (GFRP) is one approach for achieving the requirement seismic design idea of “strong-columns weak-beams”. Twelve full-scale normal-strength concrete (NC with $f_c' = 32$ MPa) and high-strength lightweight concrete (HSLWC with $f_c' = 42, 49$ and 52 MPa) exterior beam-column joints have been tested under cyclic loadings. The beams were reinforced with conventional steel bars (CS) and GFRP using steel fibers (SF). The experimental joint shear force was compared with that estimated by some international codes such as the American Concrete Institute (ACI-19), the Egyptian code (ECP-07), and the New Zealand Code (NZS-06). Nonlinear finite element analysis (ABAQUS) was carried out. In the present study, three main parameters were explored (1) HSLWC, (2) GFRP ratios equal to 0.70%, 1.03% and 1.37%, (3) SF ratios equal to 0.0%, 0.75% and 1.50%. The findings of the experiment revealed that increasing the concrete strength from NC with conventional steel bars to high-strength lightweight concrete HSLWC ($f_c' = 42$ MPa) with the same ratio of GFRP bars enhanced the first cracking load by about 25%. Increasing the SF ratio to 1.50% enhanced the failure load by 18–24% when compared with non-fiber specimens. The predicted joint shear strength estimated using the equations of the ACI 318-19 and ECP-07 are conservative for HSLWC exterior beam-column connection reinforced with GFRP bars but the predicted joint shear strength by using the equations of the NZS-07 is on the borderline for some cases. The finite element program ABAQUS can be used successfully to forecast the behavior of HSLWC beam-column connections reinforced with GFRP under seismic loadings.



Citation: El-Mandouh, M.A.; Omar, M.S.; Elnaggar, M.A.; Abd El-Maula, A.S. Cyclic Behavior of High-Strength Lightweight Concrete Exterior Beam-Column Connections Reinforced with GFRP. *Buildings* **2022**, *12*, 179. <https://doi.org/10.3390/buildings12020179>

Academic Editors: Daniele Zulli and Valeria Settmi

Received: 26 December 2021

Accepted: 30 January 2022

Published: 4 February 2022

Publisher's Note: MDPI stays neutral with regard to jurisdictional claims in published maps and institutional affiliations.



Copyright: © 2022 by the authors. Licensee MDPI, Basel, Switzerland. This article is an open access article distributed under the terms and conditions of the Creative Commons Attribution (CC BY) license (<https://creativecommons.org/licenses/by/4.0/>).

Keywords: beam-column; lightweight concrete; glass fiber reinforcement; joint shear

1. Introduction

More experimental studies are required to investigate the behavior of high-strength lightweight concrete (HSLWC) exterior beam-column joints reinforced with glass fiber bars (GFRP) under cyclic loading. Beam-column joints are the critical portions of frames due to geometric discontinuity regions. Frames composed of HSLWC and reinforced with GFRP are required for some manufacturing and car parks structures to minimize the construction weakening because of corrosion of conventional steel. The use of discrete steel fibers (SF) was introduced as a solution to improve concrete tensile strength [1], as SF has high tensile strength and proven crack-bridging capabilities. Such futures of SF can be used to change the brittle behavior of concrete, especially high strength, under tensile stress to more ductile behavior. SF reinforced concrete was also verified to be much more ductile than typical concrete under cyclic loads. Beam-column connections must be designed as geometric discontinuity zones [2]. These discontinuity regions are

not accurately designed using traditional cross-section design principles. Traditional approaches highlight the requirement for reinforcement without checking the concrete diagonal compression strength at the connection intersection zone. As structural seismic design shifts to design according to performance, it is essential to develop new structural members and systems with greater deformation capability and destruction tolerance, while only needing minor reinforcements. Connections are often exposed to considerable shear pressures throughout seismic-induced lateral displacements; this can result in serious connection damage and lack of structural stiffness [3]. ACI-ASCE Committee 352 [4] has released current design recommendations for reinforced concrete beam-column connections in earthquake-resistant construction, focusing on shear strength estimation to confirm the mechanism of the strong column-weak beam and to permit the connection to respond adequately against seismic loads. The behavior of beam-column connections has been distinguished as a major element that often becomes crucial for the global behavior of RC framed structures exposed to cyclic loads [5]. Non-conventional reinforcement, for instance, SF [6], composite materials (FRPs) [7,8], spiral reinforcement [9], and crossed inclined bars [10], have been employed to improve the structural behavior of the connections under earthquake loads. An experimental study to investigate the bond deterioration's consequences in the connection zone of interior lightweight concrete (LWC) beam-column joints was done [11]. It was found that the behavior of the LWC connections under seismic load was significantly different from that under monotonic loading because of early beam reinforcement slippage through the connection. The energy dissipated by the LWC connection was noticeably less than that of comparable normal concrete (NC) connection and the reinforcement yielded quickly due to bond collapse. The behavior of five specimens of lightweight aggregate concrete beam-column connections under monotonic loads were empirically studied [12]. The experimental outcomes highlight the necessity of proper beam-column joint reinforcement detailing, as poor detailing reduces load capacity significantly. In another experimental investigation [13] the shear strength performance of reinforced LWC beams were examined. Testing findings revealed that all the beams collapsed in the same way, because of a diagonal tension shear crack, but LWC beams showed more cracks with smaller intervals than NC specimens. Eight different exterior beam-column connections reinforced with Glass Fiber Reinforced Polymers (GFRP) bars were experimentally investigated to study the performance of the connections under seismic excitations [14]. The primary variables were concrete compressive strength, reinforcement type (GFRP bars and conventional bars), and longitudinal bars confinement. Compared to conventional connections, the connections reinforced with GFRP bars revealed lower stiffness and an elastic performance with extremely small plasticity features which caused decreased energy dissipation. In a similar study, two full-scale interior beam-column connections reinforced with GFRP were studied under seismic loads [15]. It was concluded that due to high tensile strength and low modulus of elasticity of GFRP, connections reinforced with GFRP bars can resist large side deformations under reversal cyclic loading without a sudden collapse owing to a ruptured bar. In further research, five full-scale column-beam connections reinforced with GFRP bars and stirrups were examined under simulated seismic load conditions [16] and the findings showed the possibility of utilizing GFRP bars and stirrups in connections. The results also showed that an embedment length of 24 times the GFRP bar diameter was satisfactory to transfer the forces in the beam bars to the joint under seismic loading. Two full-scale exterior T-shaped beam-column connections reinforced with GFRP bars and stirrups were investigated under simulated seismic load conditions [17] and again the results showed the feasibility of employing GFRP bars and stirrups in connections. Moreover, parallel studies [18,19] revealed that frames reinforced with GFRP can resist severe side movement. It was also suggested that [20] under cyclic excitations, frames reinforced with GFRP bars have higher strength than conventional frames. In addition, it was determined that [21] under cyclic loads, the behavior of a GFRP reinforced frame could permit larger displacements than conventional RC frames. Experimentally, six exterior beam-column connections were

seismically investigated to inspect the effect of the poor anchorage length of GFRP bars used as longitudinal reinforcement on the beam behavior [22] and it was established that the absence of anchorage length of GFRP bars in the connection considerably drop the beam's flexural strength and ductility. Recent studies [23–25] claimed that the current design codes have slight or no seismic provisions for connections reinforced with GFRP due to a shortage of data and investigations. It was also concluded that [26] additional studies are still needed to focus on other categories of connections reinforced with GFRP bars regarding the confinement provided by adjacent members. The current experimental study was performed to explore the performance of exterior LWC beam-NC column connections under seismic loads. Applying lightweight reinforced concrete beams with GFRP bars is one approach for achieving the essential design for earthquake idea of “strong-columns weak-beams”. During an extensive experimental and analytical program [27], ten exterior and ten interior beam-column joints under seismic loads have been done. The beams were constructed of lightweight concrete and reinforced with GFRP bars while the columns were constructed from NC and reinforced with conventional steel bars. The main studied parameters were the beam reinforcement ratios, beam reinforcement type (GFRP of steel), development length of the beam GFRP bars passing through the joint region, the end conditions effect of the beam GFRP bars in the exterior joints. It was revealed that a beam GFRP bar embedment length of 25 times the GFRP bar diameter inside the beam-column joint was sufficient to avoid bond deterioration of GFRP reinforced specimens. In addition, the bond between the studied lightweight concrete and the used reinforcement bars (conventional steel and GFRP) was examined by pull-out tests, and the results showed very good bond performance. The influence of steel fibers (SF) on the behavior of reinforced concrete (RC) beams with conventional steel reinforcements exposed to cyclic loading was empirically inspected [28]. The main investigated parameter was the SF content per volume. It was found that when compared to the RC beam, the SFRC beam demonstrated an enhanced seismic response and exhibited a significant flexural behavior with considerable ductility due to the capability of the SF to transfer the developed tensile stresses across cracks. In a similar investigation, eleven SFRC beams were tested experimentally and analytically under cyclic loading to investigate the advantageous effect of SF on the seismic resistance of RC beams [29]. The primary test variables were the main longitudinal steel reinforcement ratio, the stirrups reinforcement ratios, and SF volumetric proportions. The results concluded that SF enhanced the cyclic performance of the SFRC beams in terms of load-carrying capacity, the capability of energy dissipation, residual stiffness, and cracking behavior.

The primary goals of this investigation are to study experimentally and analytically the effects of using lightweight concrete; glass fiber reinforcement (GFRP) bars ratios and steel fiber (SF) ratios on the performance of exterior beam-column connections under reversal loading. A comparison between the experimental joint shear force and that calculated by some studied international codes such as the American Concrete Institute (ACI-19) [30], Egyptian code (ECP-07) [31], and the New Zealand Code (NZS-06) [32] was also carried out. Finally, to validate the experimental results, the nonlinear finite element analysis program ABAQUS [33] was carried out.

2. Experimental Program

2.1. Reinforcement

Conventional steel bars (CS) or glass fiber bars (GFRP) were used to reinforce beams of exterior connections whereas the columns were reinforced with conventional steel bars (CS). Figure 1 depicts the stress-strain curves for the bars utilized in this investigation, while Table 1 lists the parameters of the conventional steel bars and glass fiber bars employed in this study. GFRP bars' strength and rigidity are influenced by the number, type, and adjustment of glass fibers. GFRP bars demonstrate elastic behavior and are linear-elastic until fracture.

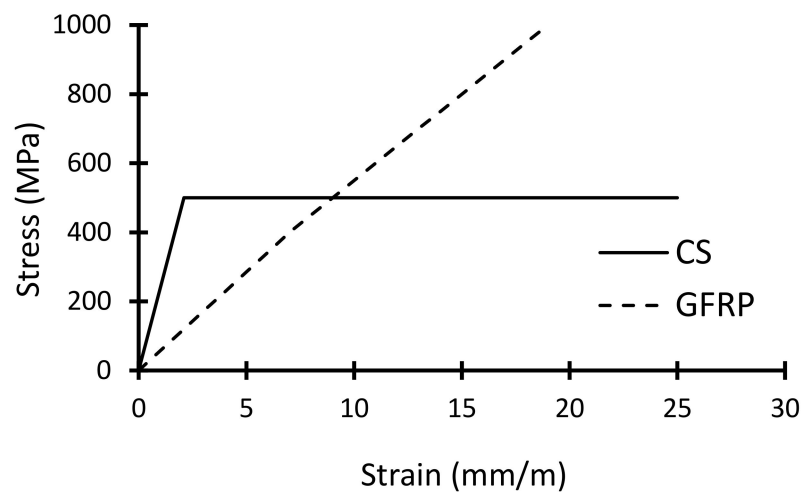


Figure 1. Stress-strain curve for GFRP and CS.

Table 1. Experimental properties of used reinforcement.

Material Properties	CS	GFRP	
Tensile strength, f_t	550	1000	MPa
Characteristic yield strength, f_y	500	-	MPa
Designed yield strength, f_{yd}	435	-	MPa
Strain yield stress, ε_y	2.18	-	mm/m
Elasticity modulus, E	2×10^5	6×10^4	MPa

2.2. Concrete Properties

Three high-strength lightweight concrete (HSLWC) mixtures and one normal concrete (NC) mixture were used. The concrete mixtures No. 1, 2 and 3 represent the concrete mixtures for HSLWC with different SF ratios (0%, 0.75% and 1.50%) while concrete mix. No. 4 represents the concrete mixture for NC without SF. Table 2 shows the concrete mixtures for both HSLWC and NC. Experimental tests for concrete cylinder compression strength (f_c'), tensile strength (f_t), and concrete modulus of elasticity (E_c) were measured on three cylinders of dimensions (150 × 300 mm) for each test [30] also, the concrete compressive cube strength (f_{cu}) were measured on three cubes (150 × 150 × 150 mm) for each mixture [31]. The total number of cubes to determine the concrete compressive cube strength was 12, where 3 cubes for each concrete mix and the total number of cylinders to determine the concrete cylinder compressive strength was 12, where 3 cylinders for each concrete mix. To determine the concrete tensile strength, a total of 12 cylinders were tested, 3 cylinders for each concrete mix. All the cubes and cylinders were tested on the same day of the test of the beam-column connection. All concrete cylinders and cubes were wet-cured in the laboratory for 7 days. Table 3 shows some mechanical properties of both NC and HSLWC mixtures. Figure 2 shows the typical compressive stress-strain curves for concrete specimens with and without SF. The fracture resistance of the concrete cylinder showed that the SF slightly enhanced the compressive strength of the concrete. On the other hand, SF showed a significant enhancement for tensile strength than the gained enhancement in compressive strength. Compared with non-fibers concrete, using 1.50% SF improved the compressive strength and tensile strength by 23% and 73%, respectively. The manufactured mechanical properties of SF as provided by the supplier are listed in Table 4 and its shape is shown in Figure 3.

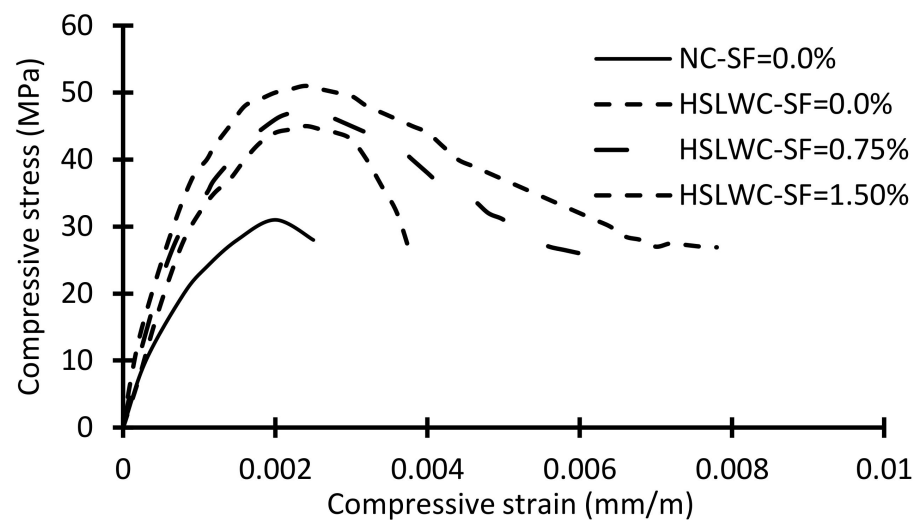
Table 2. Lightweight and normal concrete mix.

Mix. No.	Weight (Kg)								
	Cement CEMI 52.5	Silica Fume	Sand * 0/2	Liapor * 2/9E	Liapor * 6/5	Dolomite (10 mm)	Water	Super- Plasticizer	SF%
1	400	32	333	59	425	-	255	4.0	0.0
2	400	32	333	59	425	-	255	4.0	0.75
3	400	32	333	59	425	-	255	4.0	1.50
4	500	-	595	-	-	1105	215	-	0.0

*: Expanded clay aggregate.

Table 3. Mechanical properties of concrete specimens.

Mix. No.	SF%	f_c' (MPa)	St. Devia- tion	f_t (MPa)	St. Devia- tion	f_{cu} (MPa)	St. Devia- tion	E_c (MPa)	St. Devia- tion
1	0.0	42	0.07	2.29	0.07	53	0.06	25,622	0.10
2	0.75	49	0.11	2.89	0.11	61	0.10	28,000	0.11
3	1.50	51	0.13	3.97	0.12	64	0.13	27,600	0.12
4	0.0	32	0.05	2.90	0.04	40	0.04	24,890	0.08

**Figure 2.** Stress-strain curves for typical cylinder specimens.**Table 4.** Mechanical properties of the SF.

Length (mm)	Thickness (mm)	Tensile Strength (MPa)	Elastic Modulus (GPa)	Density (g/cm ³)	Elongation%	Aspect Ratio (Length/Thickness)
50	0.5	1620	42.80	1.3	7.0	100



Figure 3. Shape of SF.

2.3. Test Specimens

The cross-sections of both beams and columns were designed using a Finite Element Program (ABAQUS) [33] before the experimental work based on the Joint ACI-ASCE Committee 352 current design recommendations for RC beam-column joints in earthquake-resistant buildings [4]. The test program included twelve full-scale specimens of exterior beam-column connections bounded by the lines of contra flexure. All the specimens have the same beam dimensions (150×300 mm) with beam effective depth equal to 270 mm. The columns have a rectangular cross-section of (200×350 mm) and a height of 750 mm above and below the beams as shown in Figure 4. The columns were highly reinforced to initiate the failure in the beams (strong column-weak beam) with conventional longitudinal reinforcement bars ratio of 2.20% and all the columns were constructed from NC to simulate the newly followed techniques in buildings. During the construction of the tested specimens, the two types of concrete mixtures were poured at the same time while the samples were vertically set. First, the lower column of height 750 mm was poured by NC then the beam was cast with HSLWC, finally the upper column of height 750 mm was cast with NC. Figure 5 illustrates concrete types for specimens elements. The specimens were designed to govern the failure mechanism of the beams. Four main parameters were used in beams of specimens, (1) HSLWC with cylinder compressive strengths equal to 42, 49 and 51 MPa, (2) NC with cylinder compressive strength equal to 32 MPa, (3) top and bottom GFRP ratios equal to 0.70%, 1.03% and 1.37%, (4) SF ratios equal to 0.0%, 0.75% and 1.50%. The reference specimens BC1, BC2 and BC3 were constructed from NC with conventional steel bars CS ratios 0.70%, 1.03% and 1.37%, respectively, without SF ratio. The specimen's designations can be expressed as follows; the first two letters, BC means exterior beam-column connections. The third letter indicates the beam concrete strength (H: HSLWC with $f_c' = 42$ to 51 MPa). The fourth letter indicates the GFRP ratio (1: GFRP ratio 0.70%, 2: GFRP ratio 1.03% and 3: GFRP ratio 1.37%). The fifth letter indicates the SF ratio (0: SF ratio 0.0%, 1: SF ratio 0.75% and 2: SF ratio 1.50%). Table 5 illustrates the details of the tested exterior beam-column connections. The American code [30] specifies that under seismic loading and to accommodate the concrete deterioration attributable to cracking, the contribution of concrete to shear strength is ignored where the plastic hinge could develop. In other words, the beam transverse reinforcement is required to carry the whole shear applied to the beam section. All the columns are reinforced with conventional longitudinal bars with a diameter of 18 mm and stirrups bar diameter of 10 mm every 100 mm to achieve a strong column-weak beam. Figure 6 shows the details of the cross-section of tested beams on the faces of the columns. The end heads for GFRP bars help provide adequate anchorage as illustrated in Figures 7 and 8 illustrates GFRP bars deformations.

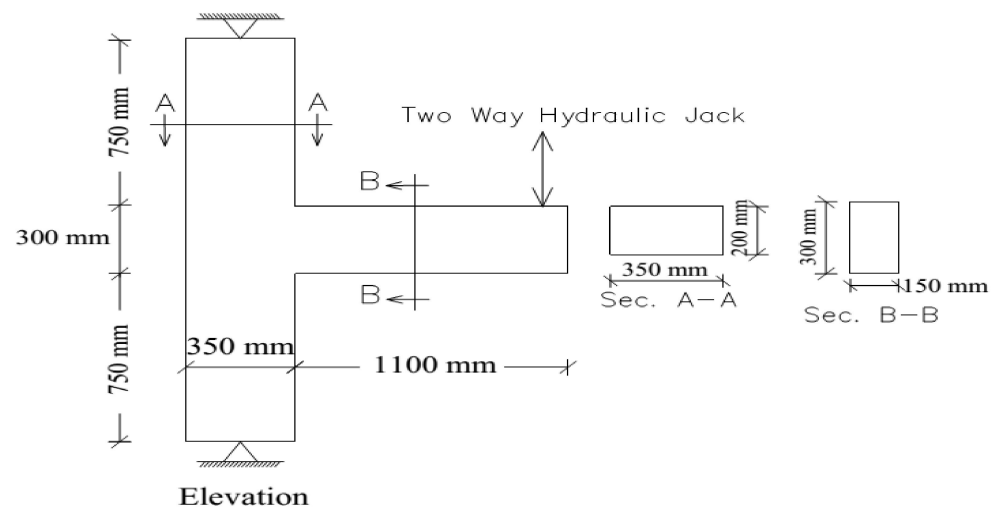


Figure 4. Dimensions of tested specimens.

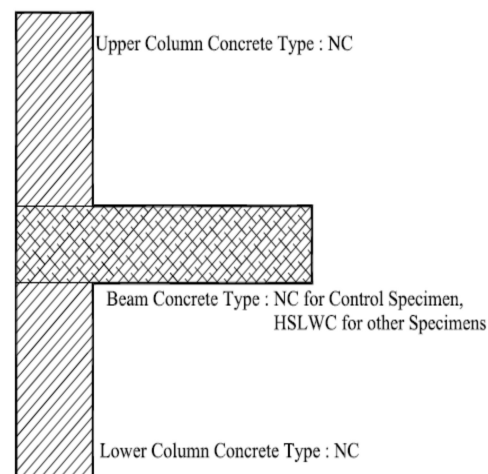


Figure 5. Concrete types for specimens' elements.

Table 5. Details of the studied exterior beam-column connections.

Specimen	Mix. No.	SF%	Beams		Column	
			Top and Bottom Bars	Stirrups (CS)	Longitudinal Bars (CS)	Stirrups (CS)
BC1 (control)	4	0.0	2D14 mm (CS)	D8 @100 mm	8D18	D10 @100 mm
BCH10	1	0.0	2G14 mm(GFRP)	D8 @100 mm	8D18	D10 @100 mm
BCH20	1	0.0	3G14 mm(GFRP)	D8 @100 mm	8D18	D10 @100 mm
BCH30	1	0.0	4G14 mm(GFRP)	D8 @100 mm	8D18	D10 @100 mm
BC2 (control)	4	0.0	3D14 mm(CS)	D8 @100 mm	8D18	D10 @100 mm
BCH11	2	0.75	2G14 mm(GFRP)	D8 @100 mm	8D18	D10 @100 mm
BCH21	2	0.75	3G14 mm(GFRP)	D8 @100 mm	8D18	D10 @100 mm
BCH31	2	0.75	4G14 mm(GFRP)	D8 @100 mm	8D18	D10 @100 mm
BC3 (control)	4	0.0	4D14 mm(CS)	D8 @100 mm	8D18	D10 @100 mm
BCH12	3	1.50	2G14 mm(GFRP)	D8 @100 mm	8D18	D10 @100 mm
BCH22	3	1.50	3G14 mm(GFRP)	D8 @100 mm	8D18	D10 @100 mm
BCH32	3	1.50	4G14 mm(GFRP)	D8 @100 mm	8D18	D10 @100 mm

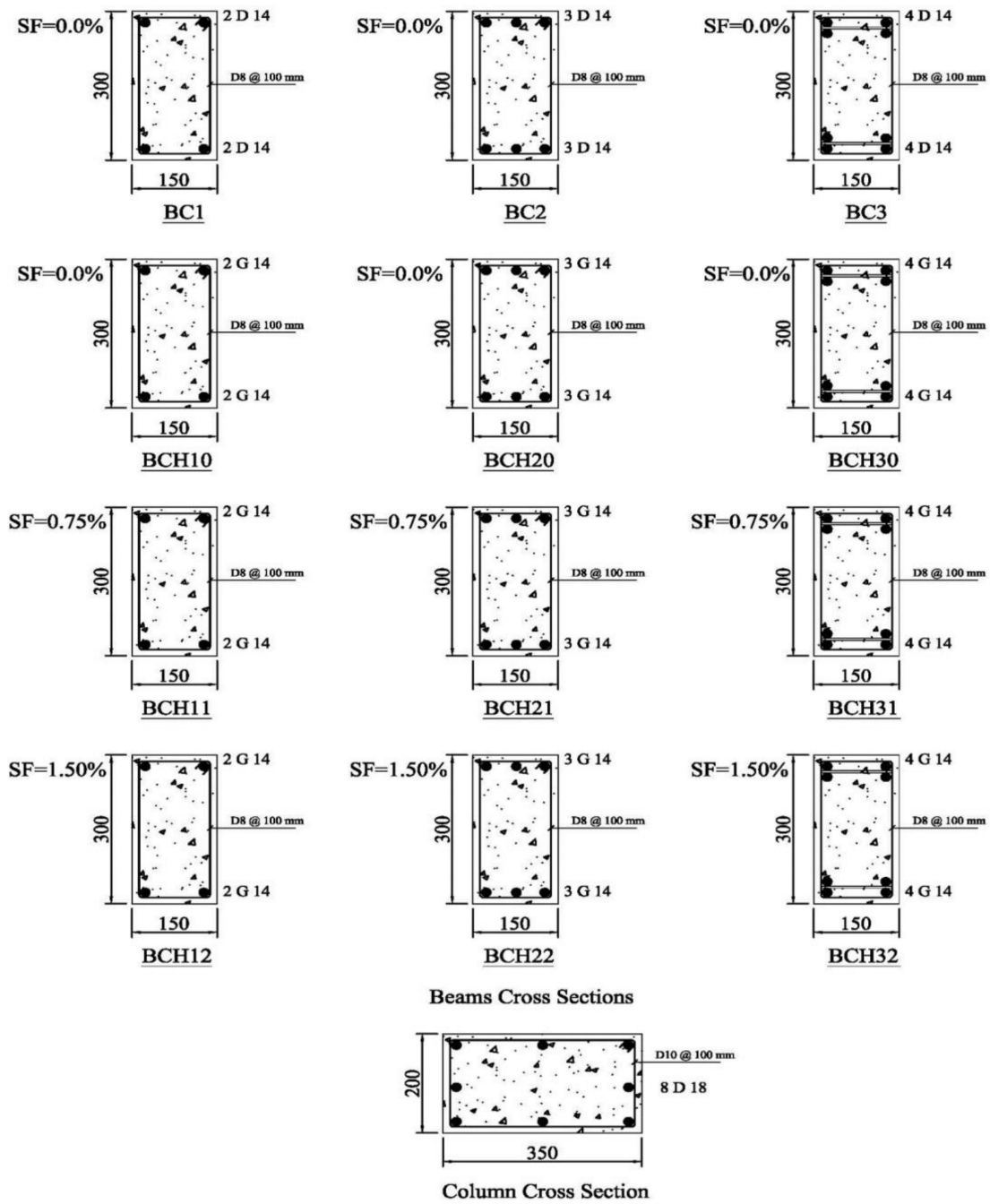


Figure 6. Details of the beam and column cross-section.



Figure 7. End heads for GFRP.

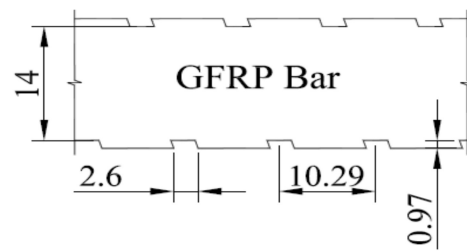


Figure 8. GFRP bar deformations (dimensions in mm).

2.4. Test Setup, Load History, and Instrumentation

Figure 9 depicts the test setup for the tested beam-column joints. The two ends of the column were restrained against both vertical and horizontal displacements whereas their rotations were allowed (hinged condition). The two-way hydraulic jack with 100-ton capacity was fixed to the end of the beam that delivers vertical cyclic loading on the specimens with a frequency of 1 cycle every 50 s, as illustrated in Figure 10. The strain gauges were used to measure the strains in the beam's top and bottom bars at the column face, column stirrups at the mid-height of joint connection, and conventional longitudinal bars of columns as shown in Figure 11. During the test, six displacement gauges (LVDTs) were located on the surface of the joint intersection to measure the rotation angle between the column and the beam and joint distortion. Figure 12 illustrates GFRP bars' head locations and LVDTs locations for bars slippage.



Figure 9. Test setup for exterior beam-column connection.

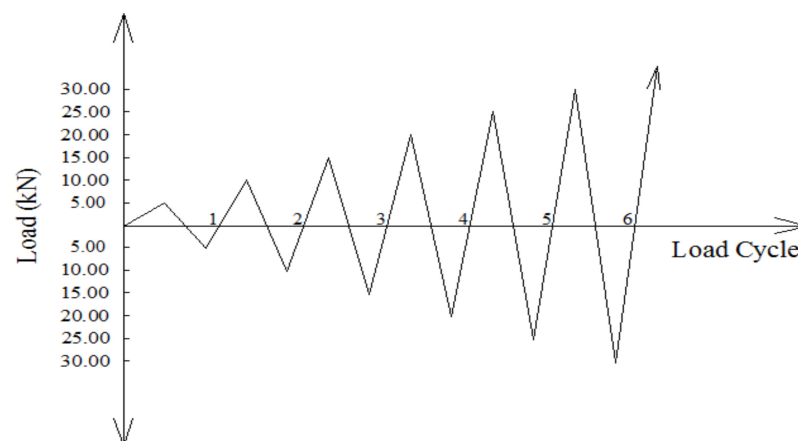


Figure 10. Lateral displacement history.

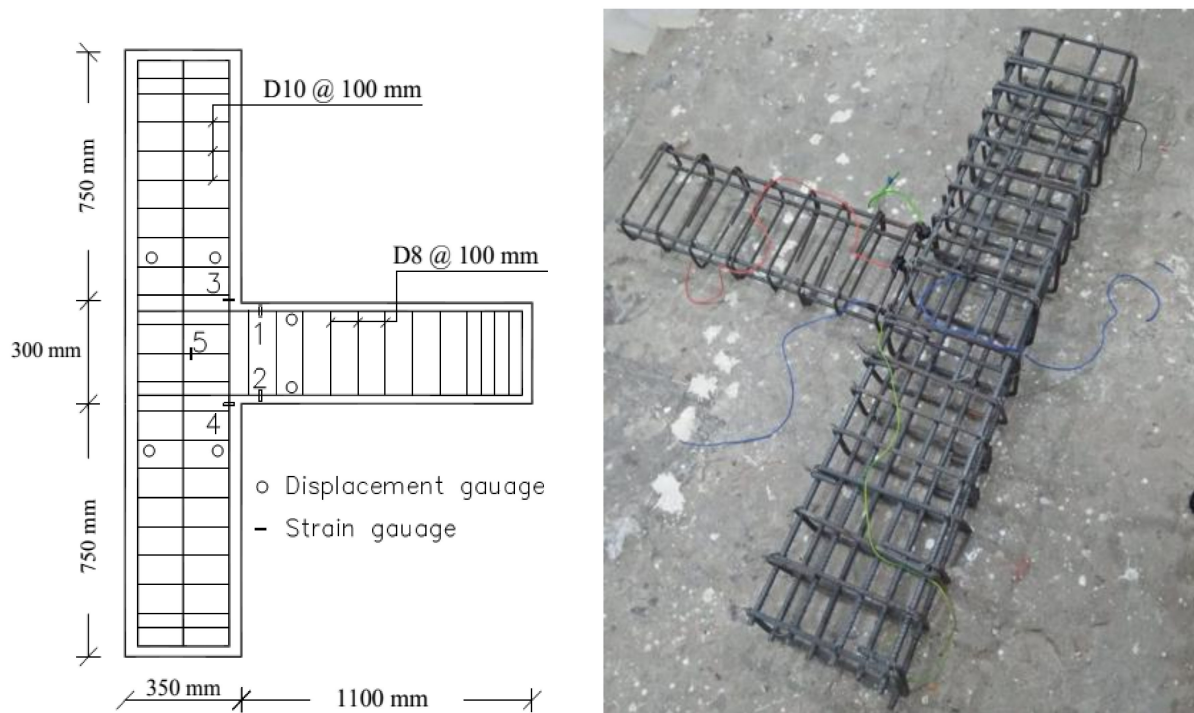


Figure 11. Displacement and strain gauges distribution for tested beam-column connection.

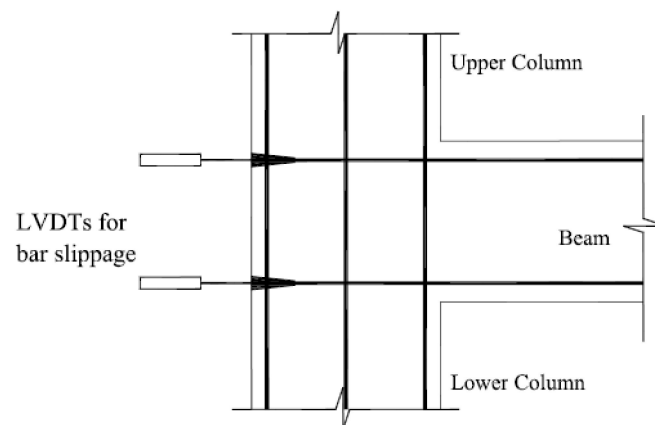


Figure 12. GFRP bars heads locations and LVDTs locations for bars slippage.

3. Experimental results and discussion

3.1. Cracking Behavior and Ultimate Strength

Figure 13 displays crack patterns for the tested specimens. All beams were visually examined until the initial crack appeared; at that point, the initial cracking load was recorded. No cracks were observed in the connection intersection area for all tested specimens. Generally, initial cracks for control specimens BC1, BC2, and BC3 were concentrated near the column at a distance equal to twice beam depth measured from the face of the column, at the location of the plastic hinge. On the other hand, for beams of the specimens reinforced with GFRP bars without SF, the flexural cracks were distributed over a longer length of the beam due to different bond characteristics of the GFRP bars compared to conventional bars. Finally, in the beams of specimens reinforced with GFRP and having SF, the flexural cracks were distributed over the longest distance of the beam due to the strain hardening tendency of SF, these fibers could withstand tension load after cracking. In comparison to non-fibrous specimens, increasing the SF content delayed the formation of the initial crack. The addition of SF to GFRP-reinforced beams increased cracking loads while reducing crack propagation.

Table 6 shows the test results that were observed. Compared with the beam of specimens BCH10, BCH20, and BCH30 increasing the SF ratio enhances reinforced concrete beam behavior in terms of first cracking load (P_{cr}) and ultimate load (P_u). Increasing the SF ratio to 0.75% enhanced the cracking load by 14–28% when compared with non-fiber specimens. Increasing the SF ratio to 1.50% improved the cracking load by 35–40% when compared with non-fiber specimens. The experimental results showed that increasing the concrete strength from NC ($f'_c = 32$ MPa) with conventional steel bars to HSLWC ($f'_c = 42$ MPa, SF = 0.0%) with the same ratio of GFRP bars (0.70%, 1.03% and 1.37%) improved the initial cracking load (P_{cr}) by about 25%. In addition, it was found that for non-fibrous specimens, increasing the GFRP bars ratio to 1.03% and 1.37% enhanced the first cracking load (P_{cr}) by 10–17% when compared with specimens with a GFRP bars ratio of 0.70%. For specimens with an SF ratio of 0.75%, increasing the GFRP bars ratio to 1.03% and 1.37% enhanced the first cracking load (P_{cr}) by 24–27% when compared with specimens with a GFRP bars ratio of 0.70%. In addition, for specimens with an SF ratio of 1.50%, increasing the GFRP bars ratio to 1.03% and 1.37% enhanced the first cracking load (P_{cr}) by 13–15% when compared with specimens with a GFRP bars ratio of 0.70%. This exhibited that the increase in the SF ratio has no significant effect on the cracking load at higher ratios of GFRP bars. According to the LVDT results, the maximum beam bars slippage for the control specimens BC1, BC2, and BC3 were 0.0261 mm, 0.0232 mm, and 0.021 mm, respectively. However, for the GFRP bars specimens, the beam bars had no slippage before failure. This implies that under cyclic loading, the end heads for GFRP bars appear to be adequate for transferring the beam bars forces to the joint.

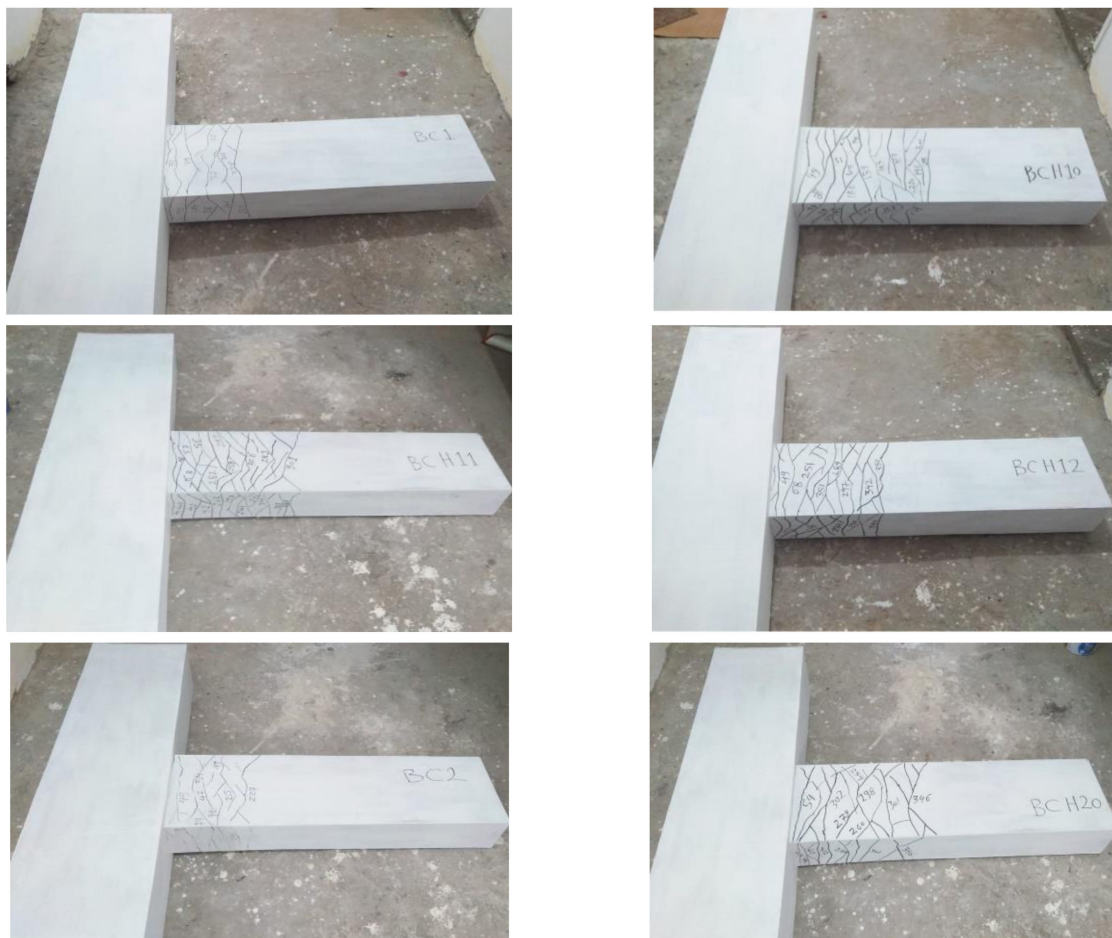


Figure 13. Cont.



Figure 13. Crack pattern of tested specimens.

Table 6. Experimental results of tested specimens.

Specimen	SF%	Experimental Test Results				
		P_{cr} (kN)	P_y (kN)	δ_L (mm)	P_u (kN)	δ_u (mm)
BC1 (control)	0	39.44	194.4	14.40	226.0	82.96
BCH10	0.0	49.3	-	18.00	282.6	103.70
BCH11	0.75	56.1	-	21.60	306.0	141.10
BCH12	1.50	68	-	21.78	351.0	145.60
BC2 (control)	0	43.52	223.2	12.96	277.9	91.12
BCH20	0.0	54.4	-	16.20	347.4	113.90
BCH21	0.75	69.7	-	18.90	390.6	142.10
BCH22	1.50	76.5	-	19.80	442.8	148.20
BC3 (control)	0	46.24	316.8	17.28	354.2	99.28
BCH30	0.0	57.8	-	21.60	442.8	124.10
BCH31	0.75	71.4	-	23.40	469.8	142.80
BCH32	1.50	78.2	-	25.20	513.0	153.00

At the ultimate level, the load-carrying capacity is enhanced for specimens reinforced with GFRP bars and containing SF. The experimental results indicated that increasing concrete strength from NC ($f_c' = 32$ MPa) with conventional steel bars to HSLWC ($f_c' = 42$ MPa, SF = 0.0%) with the same ratio of GFRP bars 0.70%, 1.03% and 1.37% enhanced the failure load (P_u) by about 25%. Increasing the SF ratio to 0.75% enhanced the failure load (P_u) by 9%, 12% and 6% for specimens BCH11, BCH21, and BCH31, respectively, when compared with non-fiber specimens. By increasing the SF ratio to 1.50% enhanced the failure load by

24%, 27% and 18% for specimens BCH12, BCH22, and BCH32, respectively, when compared with non-fibers specimens. Similarly, the results presented that increasing the GFRP bars ratio to 1.03% improved the failure load (P_u) by 23–27% when compared with specimens with a glass fiber bars ratio of 0.70%. Furthermore, increasing the glass fiber bars ratio to 1.37% enhanced the failure load (P_u) by 46–57% when compared with specimens with a GFRP bars ratio of 0.70%. Generally, the experimental results displayed an improvement for (P_{cr}) and (P_u) by increasing the GFRP bars ratio. Furthermore, the increasing of GFRP bars ratio enhanced the flexural capacity of beams containing SF.

3.2. Hysteretic Curves of Lateral Load against End Vertical Beam Displacement

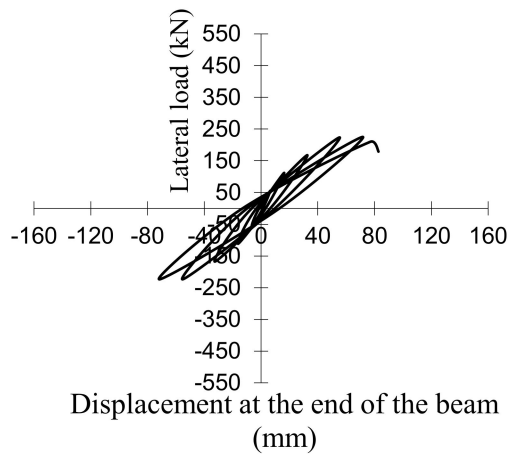
Figure 14 illustrates the hysteretic curves of cyclic load against vertical end beam displacement for all test specimens. Table 6 shows the maximum vertical displacement at the end of the beams (δ_u). Experimental outcomes showed that increasing concrete strength from NC ($f_c' = 32$ MPa) with conventional steel bars to HSLWC ($f_c' = 42$ MPa, SF = 0.0%) with the same ratio of GFRP bars (0.70%, 1.03% and 1.37%) increased the end beam displacement (δ_u) by about 25%. The maximum end vertical displacement of beams (δ_u) for specimens BCH11, BCH21 and BCH31 that contain an SF ratio of 0.75% increased by about 15%–36% when compared with non-fiber specimens. Similarly, increasing the SF ratio to 1.50% increased the beam end vertical displacement by 23–45% for specimens BCH12, BCH22, and BCH32 when compared with non-fiber specimens. Dislike, increasing the GFRP ratio to 1.03% had a minor increase in the end displacement of beams (δ_u) when compared with specimens with a GFRP bars ratio of 0.70%. Finally, increasing the GFRP bars ratio to 1.37% increased the end displacement of beams (δ_u) by 2–19% when compared with specimens with a GFRP bars ratio of 0.70%. Due to strain hardening and numerous micro-cracking characteristics of SF, beams containing SF have a higher displacement before failure, as shown in Figure 14. In addition, after unloading, the GFRP lightweight concrete beam-column connections showed minor residual deformations. The low modulus of elasticity of the GFRP bars appears to have resulted in a reduction in overall specimen stiffness, which is regarded as a benefit in terms of overall structural behavior. True, the GFRP-reinforced frame's lower rigidity will result in greater displacement, but it will also result in a longer natural period, which is inversely proportional to the design spectral acceleration. This indicates that a structure with a lower stiffness will have a lower total base shear.

The area under the envelope load-deflection curve is defined as energy absorption (I). Table 7 shows the energy absorption for tested specimens. The results showed that the energy absorption was enhanced by increasing SF ratios. By increasing SF ratio from 0.0% to 0.75–1.50%, the energy absorption was increased by 58–86% for GFRP ratio 0.70%, 39–66% for GFRP ratio 1.03%, and 20–40% for GFRP ratio 1.37%. Although the minor energy dissipation is considered a drawback, it also means that the connection regains its original shape after the loads were removed, thus requiring a minimum amount of repair after surviving such a loading event. Results found that the inclusion of beams with GFRP bars enhanced energy absorption. This could be attributed to the fact that GFRP demonstrates elastic behavior and the traditional concepts of ductility are inadequate for evaluating the ductility of concrete beams reinforced with GFRP. When utilizing GFRP in reinforced concrete structural members, both quantitative and qualitative ductility tests are required [34]. The deformability factor (μ) was defined as [34]:

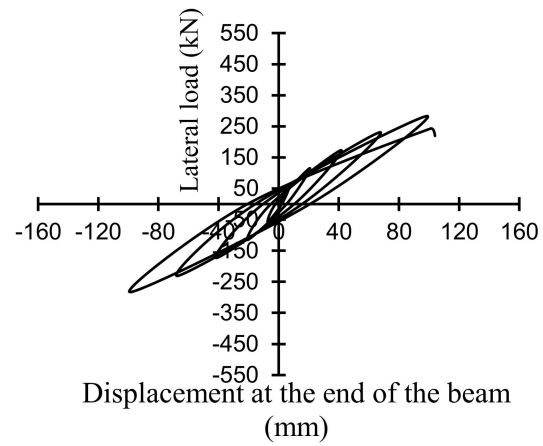
$$\mu = \delta_u / \delta_L \quad (1)$$

where δ_L is the equivalent deflection at the uncracked section. The deformability factor of the studied beams was generally improved by increasing SF ratios as illustrated in Table 7. Specimens reinforced with GFRP bars have relatively significant inelastic deformation capacity and reach extraordinary strength during post-cracking deformation. By increasing GFRP bars ratio from 0.70% to 1.03%, the deformability factor was improved by 23%, 13% and 8% for SF ratios of 0.0%, 0.75% and 1.50%, respectively. As well, by increasing GFRP

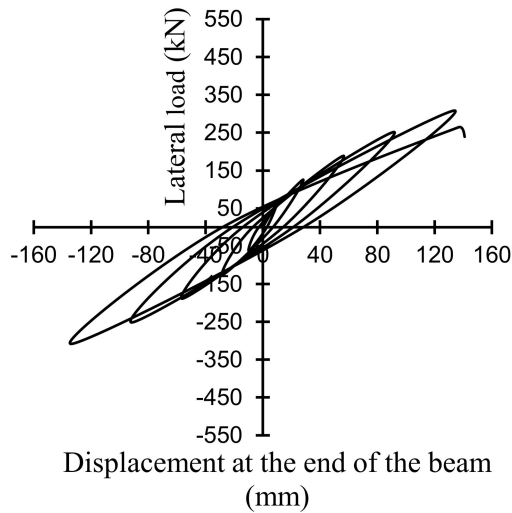
bars ratio from 0.70% to 1.37%, the deformability factor was improved by 32%, 23% and 18% for SF ratios of 0.0%, 0.75% and 1.50%, respectively.



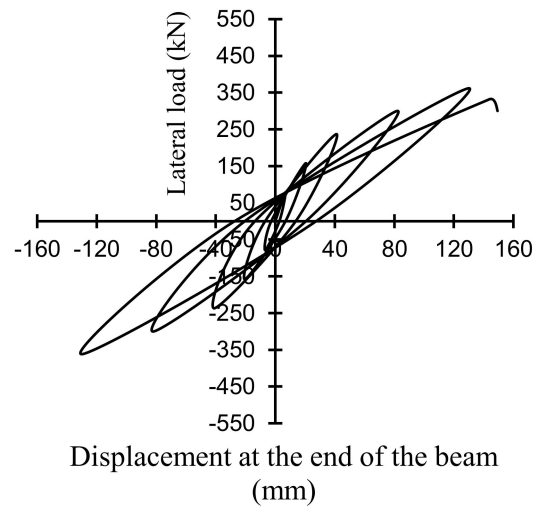
(a) Specimen BC1



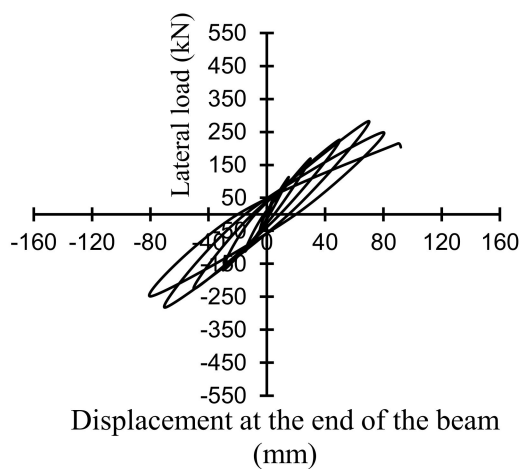
(b) Specimen BCH10



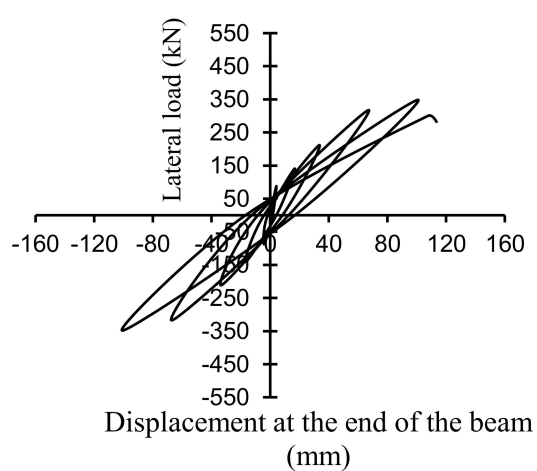
(c) Specimen BCH11



(d) Specimen BCH12

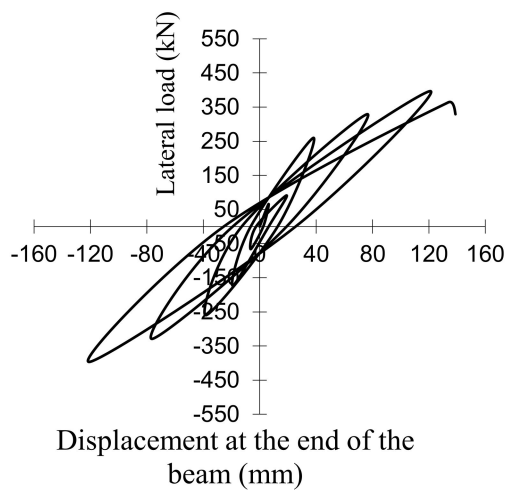


(e) Specimen BC2

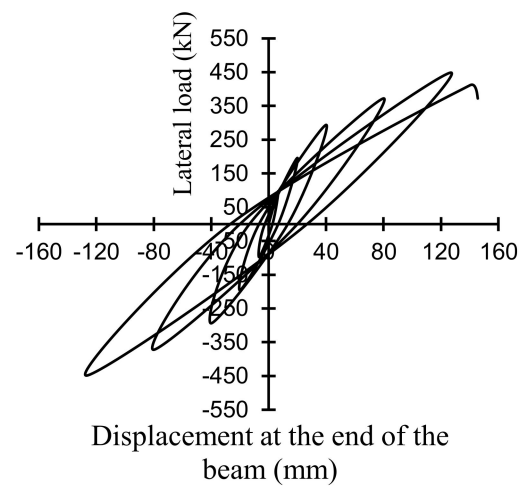


(f) Specimen BCH20

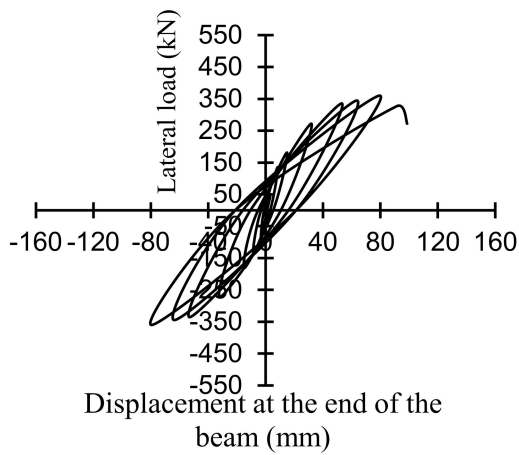
Figure 14. Cont.



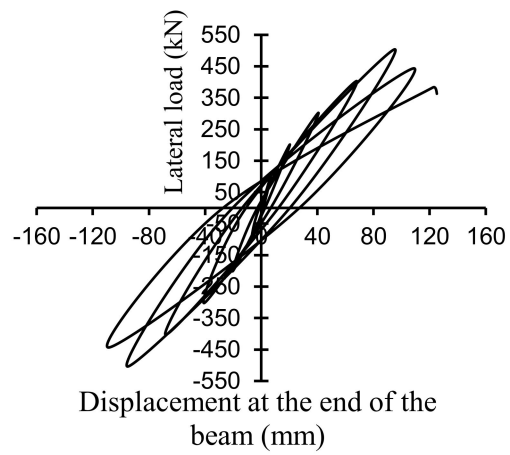
(g) Specimen BCH21



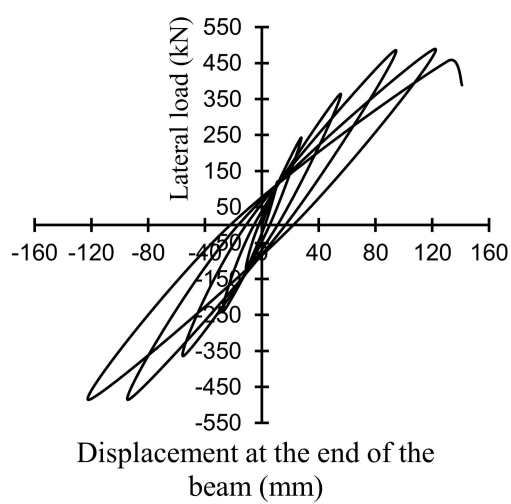
(h) Specimen BCH22



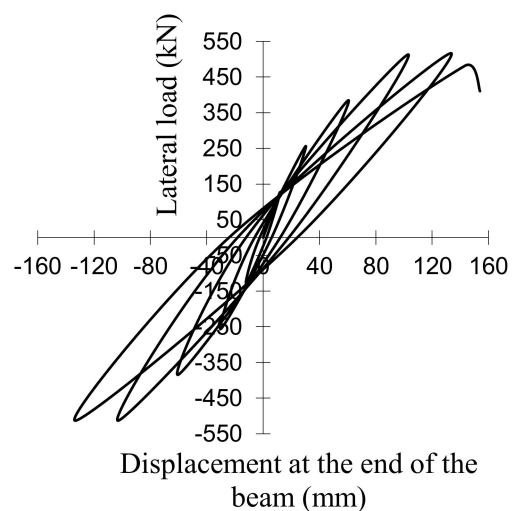
(i) Specimen BC3



(j) Specimen BCH30



(k) Specimen BCH31



(l) Specimen BCH32

Figure 14. Hysteretic loops for the tested exterior beam-column connections.

Table 7. Energy absorption, deformability factor, and maximum longitudinal beam strain results of tested specimens.

Specimen	Experimental Test Results		
	I (kN.mm)	μ	ϵ
BC1 (control)	6640	5.76	0.0241
BCH10	8300	5.72	0.0153
BCH11	13115	6.53	0.0168
BCH12	15500	6.87	0.0180
BC2 (control)	9440	7.03	0.0231
BCH20	11800	7.03	0.0112
BCH21	16400	7.38	0.0127
BCH22	19600	7.38	0.0145
BC3 (control)	13520	7.75	0.0221
BCH30	16900	7.75	0.0074
BCH31	20418	8.07	0.0090
BCH32	23600	8.10	0.0108

3.3. Strains in Bars

The maximum strain (ϵ) of CS and GFRP bars of beams at the faces of the columns was measured and recorded in Table 7. GFRP bars demonstrated elastic behavior, and they can exhibit significant elastic strains when compared to conventional steel bars. The GFRP beam bars remained linear-elastic up to failure at maximum strains, as expected. The experimental results exposed that increasing concrete strength from NC ($f'_c = 32$ MPa) with conventional steel bars to HSLWC ($f'_c = 42$ MPa, SF = 0.0%) with GFRP bars ratios 0.70%, 1.03% and 1.37%, decreased the maximum bar strain (ϵ) by 58%, 106% and 200%, respectively. This could be attributed to the stronger behavior of specimens having HSLWC against reversal loads. Additionally, the maximum bars strains were increased by increasing GFRP ratios. The results showed that by increasing SF ratios, the maximum bars strains were increased. The increase in the maximum bars strain is attributed to the existence of the steel fibers in the mass of concrete. These strain data revealed that GFRP bars deformed in the same order as conventional steel bars when specimens failed, this shows that large-elastic deformations of GFRP bars may be used to replace the yield of conventional steel bars. For all specimens, the strains in the column bars remained elastic up to failure which indicates a strong column concept was achieved. The maximum strains in the transverse reinforcement inside the joint and conventional longitudinal bars of columns for all tested specimens did not exceed its yield strength. The high deformation of beams strengthened with GFRP can be attributed to the fact that GFRP rods can withstand very significant strains before reaching their ultimate strength of 1000 MPa due to their lower modulus of elasticity.

3.4. Rotation Measurements

As shown in Figure 15, end beam displacement values can be separated into four components. These components are (1) rotation in the expected plastic hinge zone of the beam, (2) rotation attributable to large strains developed in the beam bars within the joint, (3) rotation attributable to column rotation, and lastly (4) joint distortion [16]. The rotation due to one of the main drift components was measured by each pair of LVDTs. The rotation value in radians is calculated by dividing the difference between the readings of any pair of LVDTs by the spacing between them. The plastic hinge zone in GFRP specimens is represented by the large-elastic deformation displayed by the GFRP bars, which can be referred to as a "virtual plastic hinge". For specimens reinforced with GFRP, rotation due to beam bar strains at the virtual plastic hinge zone contributed the most to the total angle, as shown in Figure 16 for some tested specimens. However, the column rotation combined with the joint distortion impact was less than 10% of the overall drift angle, but the rotation due to beam bar slippage and substantial strains in the joint was around

30–40% of the entire drift angle. All remaining rotations are most likely due to unmeasured variables i.e., beam cracks outside the anticipated plastic hinge zone. Generally, the beams constructed from high-strength lightweight concrete absorb the most energy and dissipate it as inelastic deformations.

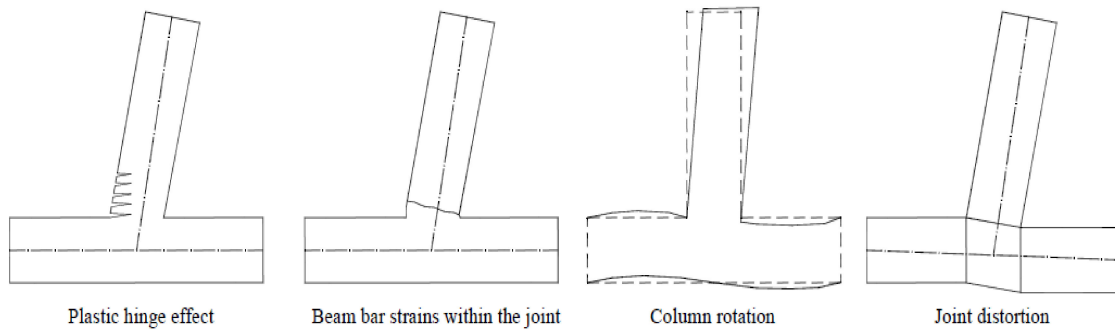


Figure 15. Main components to end beam displacement [16].

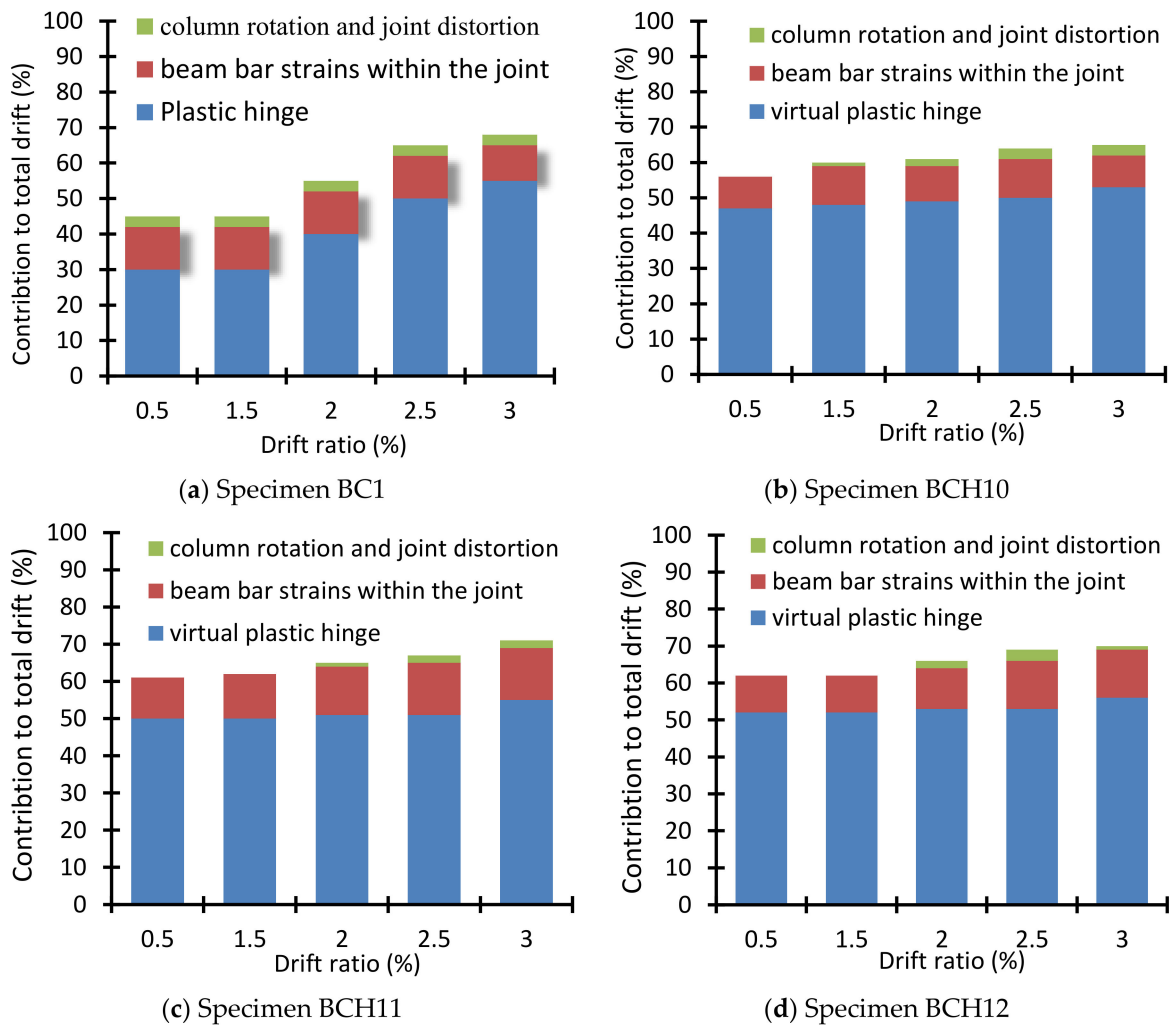


Figure 16. Cont.

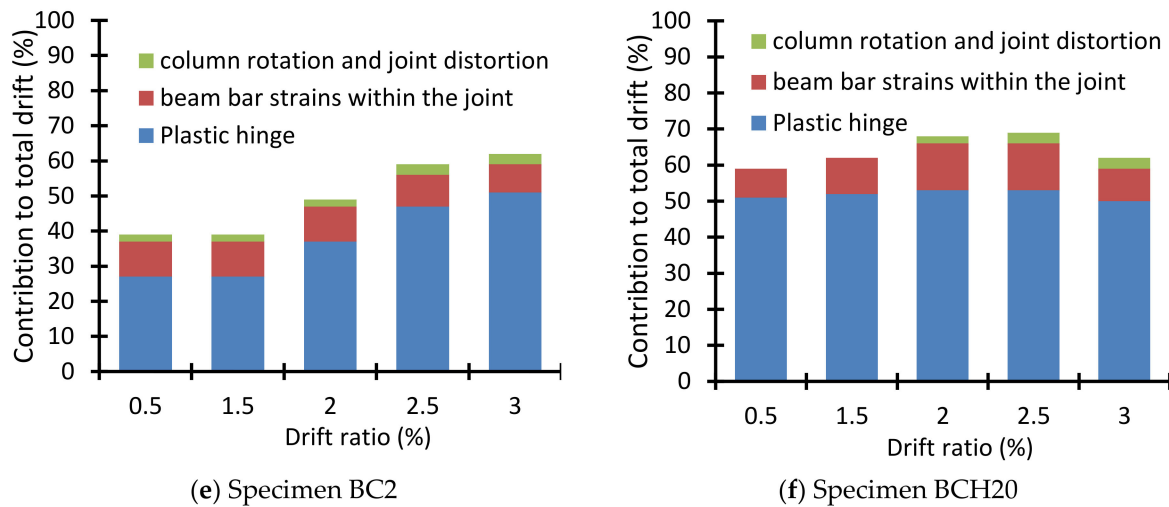


Figure 16. Percentage of contribution to total drift angle before failure for some specimens.

4. Codes Provisions

Due to the type of loading, using two different materials which are NC and HSLWC with different compressive strength and modulus of elasticity, the applicability of using studied codes for predicting joint shear shall be studied. In the current study, the joint region was constructed with NC for control specimens and HSLWC for other specimens.

4.1. ACI 318-19

The joint shear design force across a connection V_{jh} shall be taken as follows [30]:

$$V_{jh} = \lambda (f'_c)^{0.5} A_j \quad (2)$$

$$A_j = b_j h_c \quad (3)$$

$$b_j = \text{the smallest of } (b_b + 2x), (b_b + h_c), \text{ and } b_c \quad (4)$$

where λ is a factor depending on connections confined by beams and equal to 1.70, 1.20, and 1.0 for connections confined to all four faces by the beam, for connections confined to three faces by the beam, and for other cases. A_j is the effective cross-sectional area within a connection, b_j is the effective joint width, b_b is the beam width and h_c is the column depth and x is the smaller distance from beam edge to column side.

4.2. NZS-07

The joint shear design force across a connection (V_{jh}) is the least of the subsequent values [32]:

$$V_{jh} = 0.20 f'_c b_j h_c \quad (5)$$

$$V_{jh} = 10 b_j h_c \quad (6)$$

where h_c is the same as for the ACI 318-19 and b_j is the effective joint width and shall be taken the smaller of beam width, b_b or $(b_c + 0.50 h_c)$. Where b_c is the column width and b_j shall not exceed $0.50 (b_b + b_c + 0.50 h_c)$.

4.3. ECP-07

The joint shear design force across a connection (V_{jh}) is estimated from the following equation [31].

$$V_{jh} = K_j A_j (f_{cu}/\gamma_c)^{0.50} \quad (7)$$

where K_j is a factor depending on the number of beams connected by columns. A_j is the area of an effective cross-section through the joint panel and it was defined as the area

which resists shear force in load direction. f_{cu} is the cube compressive strength of concrete (MPa), γ_c is the reduction factor of concrete.

5. Test Results and Code Predictions Comparison

The joint shear strength ratio that is defined as the ratio of the experimental joint shear strength to the Code predicted joint shear strength indicates that the NZS-07 Code is the most rational one in the prediction of joint shear strength, where the average strength ratio was 1.03 and the standard deviation was 0.18. In addition, ACI 318-19 Code could be considered reasonable in the prediction of joint shear strength, where the average strength ratio was 1.13 and the standard deviation was 0.20. However, ECP-07 Code could be considered less rational as the average strength ratio was 1.36 and the standard deviation was 0.36. Table 8 shows the comparison of the experimental joint shear strength (V_{jhE}) of the specimens with nominal predictions obtained using studied international codes. This comparison illustrates that the predicted joint shear strength estimated using the equations of the ACI 318-19 and ECP-07 are conservative for HSLWC exterior beam-column connection reinforced with GFRP bars but the predicted joint shear strength by using the equations of the NZS-07 is on the borderline for some cases.

Table 8. Contrast between the experimental joint shear and that predicted by studied international codes.

Specimen	Experimental Joint Shear Strength V_{jhE} (kN)	Predicted Joint Shear Strength According to Studied International Codes V_{jh} (kN)					
		ACI 318-19	Exp./Code	NZS-07	Exp./Code	ECP-07	Exp./Code
BC1 (control)	169.5	208.6	0.81	183.685	0.92	190.2	0.89
BCH10	211.95	239.1	0.89	263.415	0.80	195.2	1.09
BCH11	229.5	239.1	0.96	263.415	0.87	195.2	1.18
BCH12	263.25	239.1	1.10	263.415	1.00	195.2	1.35
BC2 (control)	208.425	208.6	1.00	183.685	1.13	190.2	1.10
BCH20	260.55	258.3	1.01	307.36	0.85	210.9	1.24
BCH21	292.95	258.3	1.13	307.36	0.95	210.9	1.39
BCH22	332.1	258.3	1.29	307.36	1.08	210.9	1.57
BC3 (control)	265.65	208.6	1.27	183.685	1.45	190.2	1.40
BCH30	332.1	263.2	1.26	319.855	1.04	215	1.54
BCH31	352.35	263.2	1.34	319.855	1.10	215	1.64
BCH32	384.75	263.2	1.46	319.855	1.20	215	1.79
		Average	1.13	Average	1.03	Average	1.35
		st. deviation	0.20	st. deviation	0.18	st. deviation	0.26

6. Finite Element Analyses

6.1. Modeling Using Finite Elements

The behavior of HSLWC beam-column connections reinforced with GFRP was investigated using a 3D nonlinear Finite Element analysis utilizing the program ABAQUS [33]. To establish a good stress distribution in the 3D analysis, the concrete section of the model is separated into so-called brick elements using the C3D8R element. The reinforcement is treated as embedded bars.

6.2. Reinforcement

For modeling column and beam reinforcement, longitudinal reinforcement, and stirrups, the element T3D2 is used, and this 3D element is defined by two nodes having two degrees of freedom at each node. The Poisson ratio was equal to 0.30. The yield strength of

reinforcement bars was taken from experimental results. The bond between the concrete and bars reinforcement was assumed to be perfect.

6.3. Concrete

For modeling concrete, the element C3D8R is used. The element is made up of eight nodes, each of which has three degrees of freedom and can translate into the x , y , and z dimensions. The concrete damage plasticity model was used to simulate the concrete behavior as it defined the compression and tension degradation for concrete. When the element plasticizes, the damaged property reduces the elastic stiffness. It is unable to regain its initial strength, which is critical for cyclic loading. The mechanical properties of concrete were taken from experimental results. The compressive uniaxial stress-strain values for both the ascending and descending portions of the NC and HSLWC concrete model were used from experimental results.

6.4. The Finite Element Mesh

To achieve correct results, the mesh size of all the elements in the finite element model was purposefully set to the same to ensure that no two materials share the same node. The mesh element for concrete is a 3D solid element C3D8R, with a size of $25 \times 25 \times 25$ mm. The reinforcement was treated as emended bar element with mesh 25×25 mm. Figure 17 shows the concrete volume meshes and reinforcing meshes for one of the tested beam-column specimens.

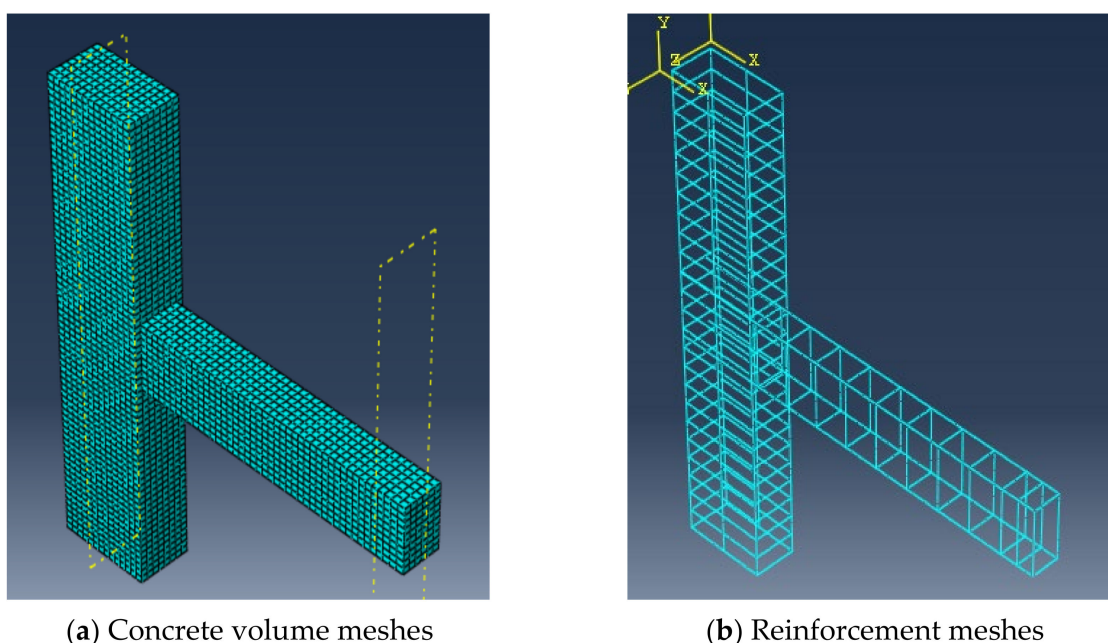


Figure 17. Boundary Conditions.

To simulate the experimental test setup, loading and boundary conditions were applied to the beam-column connections model, as illustrated in Figure 18. The ends of the columns were hinged $u_1 = u_2 = u_3 = 0.0$. The free end of the beam was loaded by cyclic loading to simulate the exterior beam-column connections under earthquake loading.

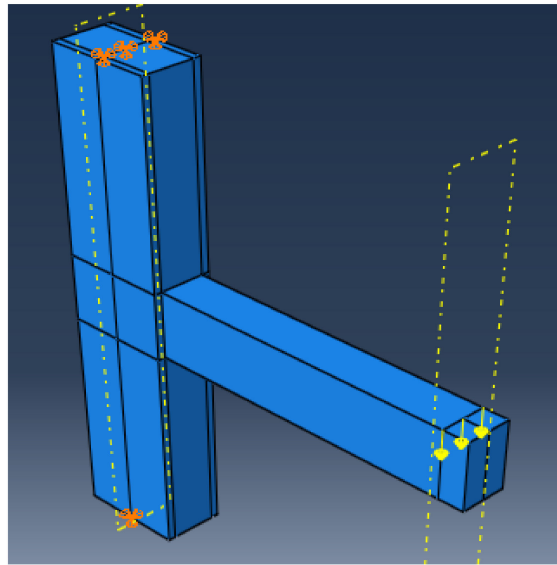


Figure 18. Comparison of the Test Results with the Predictions of the Finite Elements.

A similarity was observed between the pattern of the cracks of the experimental and finite elements. Figures 19–22 show the crack pattern of some analyzed specimens. Table 9 compares the experimental peak vertical load values with those computed using the finite element method. The comparison shows that there is a difference of about 13%, between the theoretical and the experimental failure load. Table 9 also compares the experimental maximum displacement at the end of the beam to the calculated maximum displacement using the finite element method. Figures 23–26 show the comparison between the experimental hysteretic loop for some specimens and that calculated from analytical. The results reveal that the finite element results and the experimental measurements are in good agreement. In general, the finite element program ABAQUS can be used successfully to forecast the behavior of HSLWC beam-column connections reinforced with GFRP under cyclic loadings.

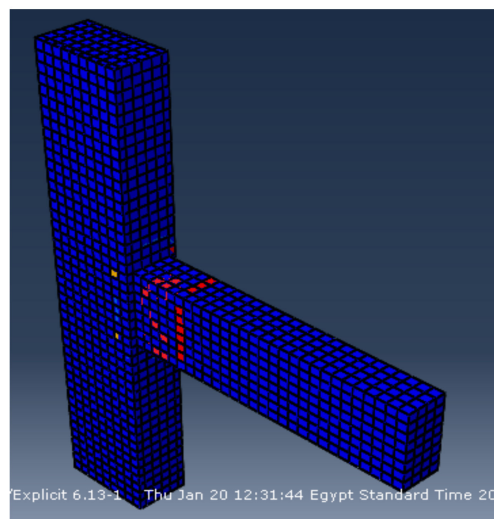


Figure 19. Final crack pattern of specimen DC1 (Analytical).

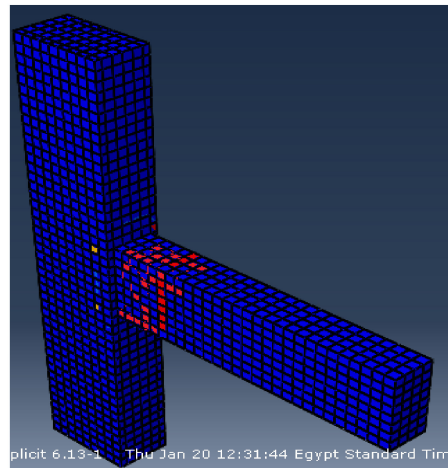


Figure 20. Final crack pattern of specimen BCH10 (Analytical).

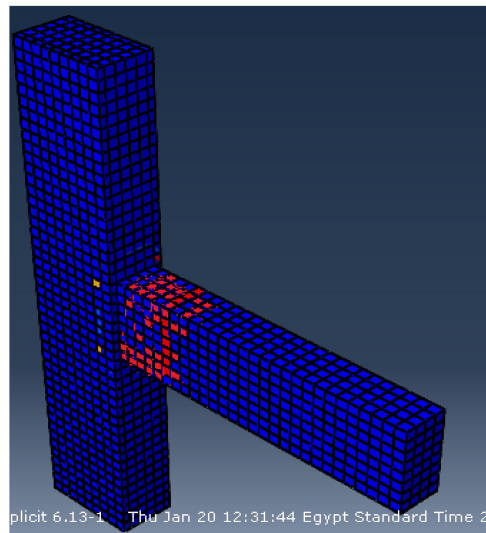


Figure 21. Final crack pattern of specimen BCH11 (Analytical).

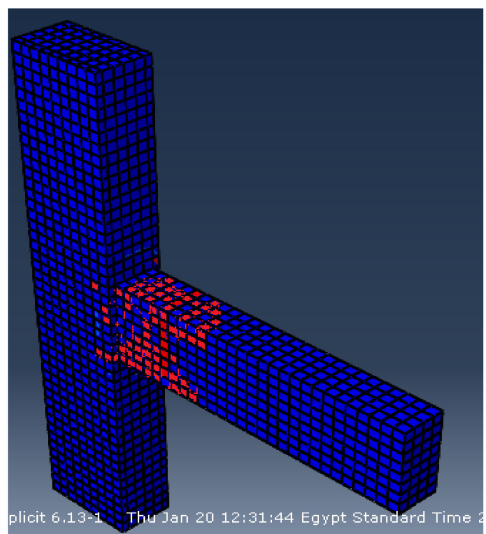
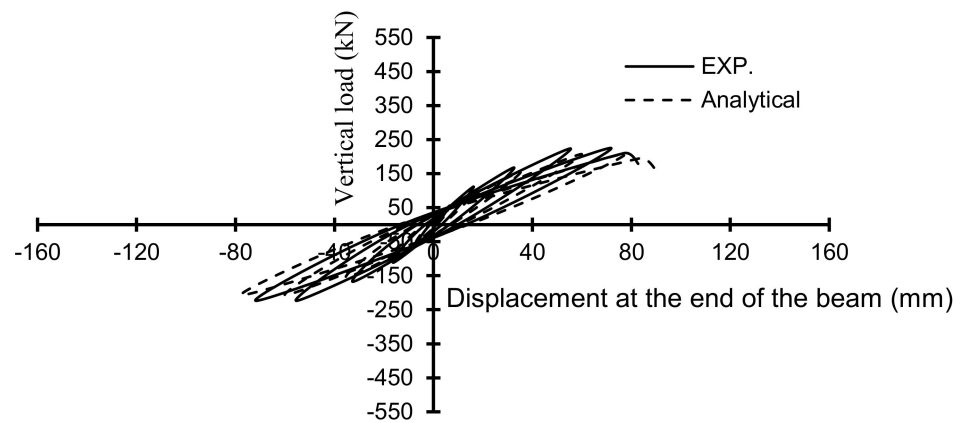
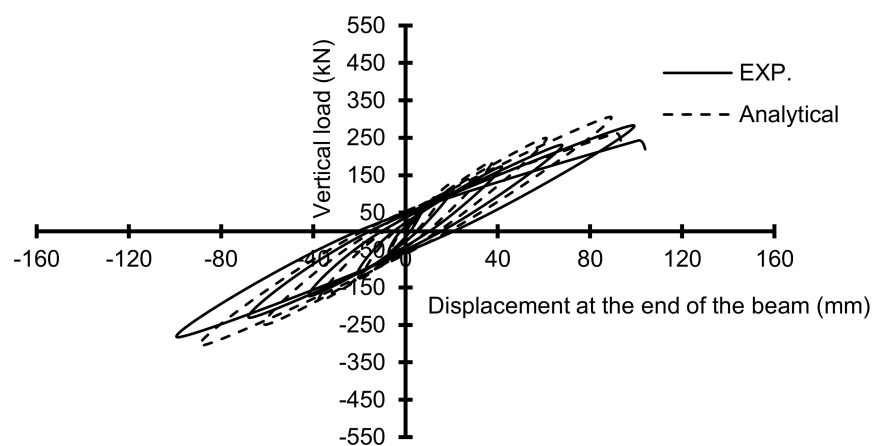


Figure 22. Final crack pattern of specimen BCH12 (Analytical).

Table 9. Comparison between the experimental and finite element results.

Specimen	Failure Load, kN		Maximum End Beam's Vertical Displacement Just Before Failure (mm).	
	Finite Element	EXP./Finite Element	Finite Element	EXP./Finite Element
BC1 (control)	209	1.08	89	0.92
BCH10	256	1.10	117	0.88
BCH11	268	1.14	169	0.83
BCH12	297	1.18	175	0.85
BC2 (control)	245	1.13	105	0.86
BCH20	324	1.07	132	0.85
BCH21	378	1.03	171	0.81
BCH22	420	1.05	175	0.83
BC3 (control)	340	1.04	120	0.82
BCH30	384	1.15	144	0.86
BCH31	390	1.20	159	0.89
BCH32	438	1.17	180	0.85

**Figure 23.** Comparison between experimental hysteretic loop for specimen DC1 and that calculated from analytical.**Figure 24.** Comparison between experimental hysteretic loop for specimen DCH10 and that calculated from analytical.

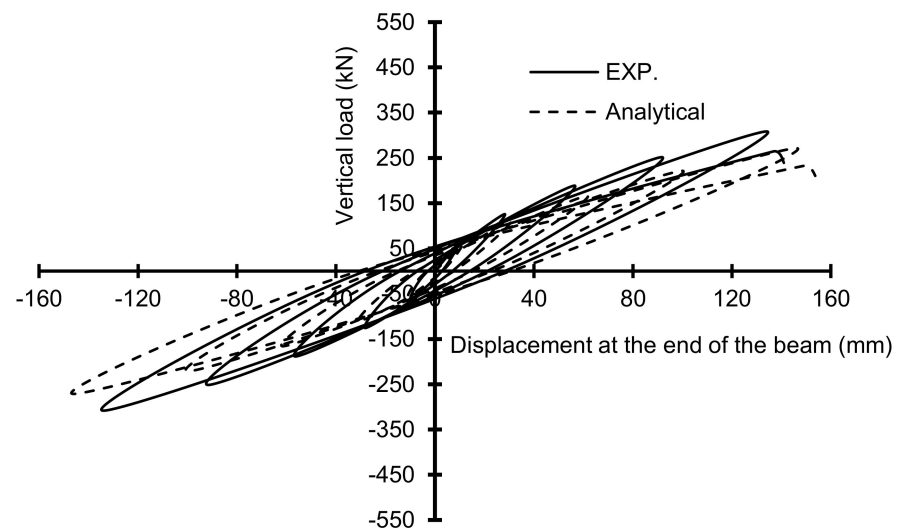


Figure 25. Comparison between experimental hysteretic loop for specimen DCH11 and that calculated from analytical.

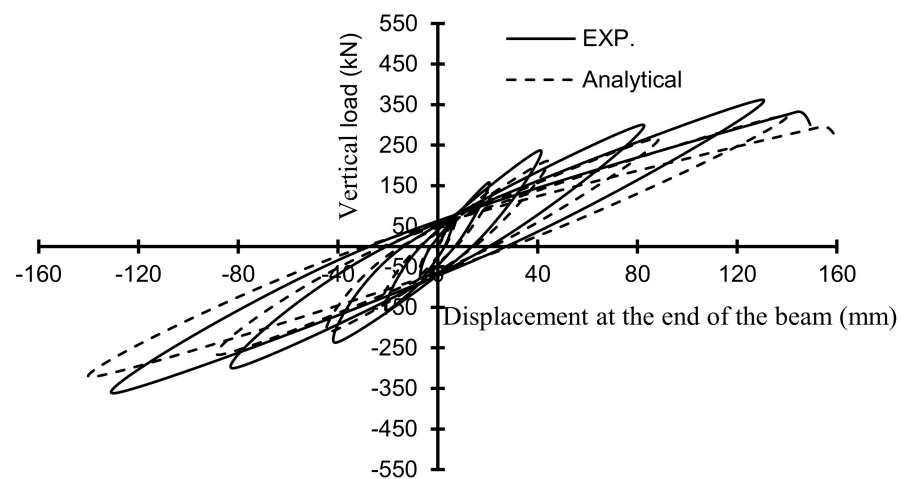


Figure 26. Comparison between experimental hysteretic loop for specimen DCH12 and that calculated from analytical.

7. Conclusions

Generally, using GFRP bars in the exterior beam-column joints as flexural bars in the connected beam enhanced the ultimate strength and ductility of the joint when compared with the conventional steel reinforcement bars. Providing SF for specimens having GFRP bars also enhanced the deformability factor than specimens with no SF.

Specimens with high GFRP bars ratio exhibited stronger behavior against cyclic loading, so the increase in SF ratios for these specimens had no significant effect.

That by increasing GFRP bars ratio the specimens exhibited stronger behavior against cyclic loading.

After unloading, the glass-fiber-reinforced lightweight concrete beam-column joints showed minor residual deformations.

Increasing the steel fiber ratio to 0.75% enhanced the cracking load by 14–28% when compared with non-fiber specimens; also, increasing the steel fiber ratio to 1.50% enhanced the cracking load by 35–40% when compared with non-fiber specimens.

Increasing the concrete strength from NC ($f_c' = 32$ MPa) with conventional steel bars to high strength lightweight concrete HSLWC ($f_c' = 42$ MPa) with the same ratio of glass fiber bars enhanced the first cracking load by about 25%.

Increasing the steel fiber ratio to 0.75% enhanced the failure load by 6–12% when compared with non-fiber specimens; also, increasing the steel fiber ratio to 1.50% enhanced the failure load by 18–27% when compared with non-fiber specimens.

Rotation caused by beam bar strains at the virtual plastic hinge zone contributed the most to the total angle for specimens reinforced with GFRP.

The predicted joint shear strength estimated using the equations of the ACI 318-19 and ECP-07 are conservative for HSLWC exterior beam-column joint reinforced with GFRP bars but the predicted joint shear strength by using the equations of the NZS-07 is on the borderline for some cases.

The finite element program ABAQUS can be used successfully to forecast the behavior of HSLWC beam-column joints reinforced with GFRP under seismic loadings.

Author Contributions: Conceptualization, M.A.E.-M. and A.S.A.E.-M.; methodology, M.A.E.-M., software, A.S.A.E.-M.; validation, M.A.E.-M., A.S.A.E.-M.; formal analysis, M.A.E.-M.; investigation, M.S.O.; resources, M.A.E.; data curation, M.A.E.-M. and A.S.A.E.-M.; writing-original draft preparation, A.S.A.E.-M., writing-review and editing, A.S.A.E.-M. and M.A.E.; visualization, M.S.O.; supervision, M.A.E.; project administration. All authors have read and agreed to the published version of the manuscript.

Funding: This research received no external funding.

Institutional Review Board Statement: Not applicable.

Informed Consent Statement: Not applicable.

Data Availability Statement: All the data supporting reported results can be found in the manuscript.

Conflicts of Interest: The authors declare no conflict of interest.

References

1. Abbass, A.; Abid, S.; Ozakça, M. Experimental Investigation on the Effect of Steel Fibers on the Flexural Behavior and Ductility of High-Strength Concrete Hollow Beams. *J. Adv. Civ. Eng.* **2019**, *2019*, 1–13. [\[CrossRef\]](#)
2. Schlaich, J.; Schäfer, K. *Konstruieren im Stahlbetonbau, Beton Kalender, Part 2*; Ernest and Son: Berlin, Germany, 2001; pp. 311–492, ISBN 9783433015834.
3. Gustavo, J.; Parra, M.; Sean, W.P.; Shih-Ho, C. Highly Damage-Tolerant Beam-Column Joints Through Use of High-Performance Fiber-Reinforced Cement Composites. *ACI Struct. J.* **2005**, *102*, 487–495.
4. ACI-ASCE Joint Committee 352. *Recommendations for Design of Beam-Column Joints in Monolithic Reinforced Concrete Structures*; American Concrete Institute: Farmington Hills, MI, USA, 2019; p. 37.
5. Chalioris, C.E.; Favvata, M.J.; Karayannis, C.G. Reinforced Concrete Beam-Column Joints with Crossed Inclined Bars under Cyclic Deformations. *Earthq. Eng. Struct. Dyn. J.* **2008**, *37*, 881–897. [\[CrossRef\]](#)
6. Shannag, M.J.; Abu-Dyya, N.; Abu-Farsakh, G. Lateral Load Response of High Performance Fiber Reinforced Concrete Beam-Column Joints. *Constr. Build. Mater. J.* **2005**, *19*, 500–508. [\[CrossRef\]](#)
7. Ghobarah, A.; Said, A. Seismic Rehabilitation of Beam-Column Joints Using FRP Laminates. *J. Earthq. Eng.* **2001**, *5*, 113–129. [\[CrossRef\]](#)
8. Karayannis, C.G.; Sirkelis, G.M. Effectiveness of RC Beam-Column Connections Strengthening Using Carbon-FRP Jackets. In Proceedings of the 12th European Conference on Earthquake Engineering, London, UK, 9–13 September 2002; p. 549.
9. Karayannis, C.G.; Sirkelis, G.M. Response of Columns and Joints with Spiral Shear Reinforcement. In Proceedings of the 12th Computational Methods and Experimental Measurements (CMEM), Wessex Institute of Technology, Malta, 20–22 June 2005.
10. Paulay, T.; Park, R. *Joints in Reinforced Concrete Frames Designed for Earthquake Resistance: A Report Prepared for a US-New Zealand-Japan Seminar, 30 July–1 August 1984, Monterey, California*; Department of Civil Engineering, University of Canterbury: Christchurch, New Zealand, 1948.
11. Bertero, V.V.; Popov, E.P.; Forzani, B. Seismic Behavior of Lightweight Concrete Beam-Column Subassemblages. *ACI J.* **1980**, *87*, 44–52.
12. Ricardo, N.F.; Hugo, C.; Gonçalo, G.; Onatas, V. Experimental evaluation of lightweight aggregate concrete beam-column joints with different strengths and reinforcement ratios. *Struct. Concr.* **2017**, *18*, 1–12.
13. Nawaz, W.A.; Abdalla, J.A.; Hawileh, R.A.; Alajmani, H.S. Experimental study on the shear strength of reinforced concrete beams cast with Lava lightweight aggregates. *Arch. Civ. Mech. Eng.* **2019**, *19*, 981–996. [\[CrossRef\]](#)
14. Azariani, H.R.; Shariatmadar, H.; Esfahani, M.R. Exterior Concrete Beam-Column Connection Reinforced with Glass Fiber Reinforced Polymers (GFRP) Bars Under Cyclic Loading. *AUT J. Civ. Eng.* **2018**, *2*, 161–176. [\[CrossRef\]](#)

15. Ghomi, S.J.; El-Salakawy, E.F. Seismic Performance of Interior GFRP-RC Beam-Column Joints. In Proceedings of the 13th International Symposium on Fiber-Reinforced Polymer Reinforcement for Concrete Structures, Anaheim, CA, USA, 15–19 October 2017; ACI Special Publication; American Concrete Institute: Farmington, MI, USA, 2017; pp. 163–180.
16. Mady, M.; El-Ragaby, A.; El-Salakawy, E.F. Seismic Behavior of Beam-Column Joints Reinforced with GFRP Bars and Stirrups. *J. Compos. Constr.* **2011**, *6*, 875–886. [[CrossRef](#)]
17. Mady, M.; El-Ragaby, A.; El-Salakawy, E.F. Experimental Investigation on the Seismic Performance of Beam-Column Joints Reinforced with GFRP Bars. *J. Earthq. Eng.* **2011**, *15*, 7798. [[CrossRef](#)]
18. Sharbatdar, M.K.; Saatcioglu, M.; Benmokrane, B. Seismic Flexural Behavior of Concrete Connections Reinforced with CFRP Bars and Grids. *J. Compos. Struct.* **2011**, *93*, 2439–2449. [[CrossRef](#)]
19. Ghomi, S.J.; El-Salakawy, E.F. Seismic Behavior of Exterior GFRP-RC Beam-Column Connections. *J. Compos. Constr.* **2018**, *22*, 1–13. [[CrossRef](#)]
20. Mamaghani, M.A.; Khaloo, A. Seismic Behavior of Concrete Moment Frame Reinforced with GFRP Bars. *J. Compos. Part B Eng.* **2019**, *163*, 324–338. [[CrossRef](#)]
21. Hopartean, G.; Donchev, T.; Petkova, D.; Costas, G.; Mukesh Limbachiya, M.; Parnada, N. Experimental Testing of Medium Scale GFRP Reinforced Concrete Frames. *Issue MATEC Web Conf.* **2019**, *289*, 04004. [[CrossRef](#)]
22. Yang, K.H.; Mun, J.H. Cyclic Flexural and Shear Performances of Beam Elements with Longitudinal Glass Fiber Reinforced Polymer (GFRP) Bars in Exterior Beam-Column Connections. *J. Appl. Sci.* **2018**, *8*, 2353. [[CrossRef](#)]
23. Hasaballa, M.; El-Salakawy, E.F. Anchorage Performance of GFRP Headed and Bent Bars in Beam-Column Joints Subjected to Seismic Loading. *J. Compos. Constr.* **2018**, *22*, 1–14. [[CrossRef](#)]
24. Ghomi, S.J.; El-Salakawy, E.F. Effect of Geometrical Configuration on Seismic Behavior of GFRP-RC Beam-Column Joints. *J. Adv. Concr. Constr.* **2020**, *9*, 313–326. [[CrossRef](#)]
25. Gajendra; Kulkarni, D.K. K. Seismic Evaluation of Beam-Column Joints Using GFRP Bars in Multi-Story Building Using Etabs. *Int. Res. J. Eng. Technol. (IRJET)* **2015**, *2*, 91–95.
26. Hasaballa, M.; El-Salakawy, E.F. Shear Capacity of Exterior Beam-Column Joints Reinforced with GFRP Bars and Stirrups. *J. Compos. Constr.* **2016**, *20*, 1–13. [[CrossRef](#)]
27. El-Zareef, M.A.M. Conceptual and Structural Design of Buildings made of Lightweight and Infra-Lightweight Concrete. Master's Thesis, Technische University, Berlin, Germany, 2010.
28. Chalioris, C.E.; Kosmidou, P.M.K.; Karayannis, C.G. Cyclic Response of Steel Fiber Reinforced Concrete Slender Beams: An Experimental Study. *Materials* **2019**, *12*, 1398. [[CrossRef](#)] [[PubMed](#)]
29. Kytinou, V.K.; Chalioris, C.E.; Karayannis, C.G.; Elenas, A. Effect of steel fibers on the hysteretic performance of concrete beams with steel reinforcement-Tests and analysis. *Materials* **2020**, *13*, 2923. [[CrossRef](#)] [[PubMed](#)]
30. American Concrete Institute. *Building Code Requirements for Reinforced Concrete, ACI318-99*; American Concrete Institute: Detroit, MI, USA, 2019.
31. Ministry of Housing and Development, Housing and Building National Research Centre. *Egyptian Code of Practice for Design and Construction of Concrete Structures, ECP-RC*; Ministry of Housing and Development, Housing and Building National Research Centre: Cairo, Egypt, 2007.
32. *STANDARDS NEW ZEALAND (NZS 3101)*; Concrete Structures Standard-Amendment 1, 2 and 3; Standards New Zealand: Wellington, New Zealand, 2017.
33. Dassault Systems Corp. *ABAQUS: Abaqus Analysis User's Manual, Version 6.9*; Dassault Systems Corp: Providence, RI, USA, 2014.
34. Newman, J.B. *Properties of Structural Lightweight Concrete in Structural Lightweight Concrete*; Clarke, J.L., Ed.; Chapman & Hall: London, UK, 1993; pp. 19–44.